7 Some Specific Laser Systems

7.0 INTRODUCTION

The pumping of the atoms into the upper laser level is accomplished in a variety of ways, depending on the type of laser. In this chapter we will review some of the more common laser systems and in the process describe their pumping mechanisms. The laser systems described include: ruby, Nd^{3+}:YAG, Nd^{3+}:glass, He–Ne, CO_2, Ar^+, excimer, and organic-dye lasers.

7.1 PUMPING AND LASER EFFICIENCY

Figure 7-1 shows the pumping–oscillation cycle of some (hypothetical) representative laser. The pumping agent elevates the atoms into some excited state 3 from which they relax into the upper laser level 2. The stimulated laser transition takes place between levels 2 and 1 and results in the emission of a photon of frequency ν_{21}.

It is evident from this figure that the minimum energy input per output photon is $h\nu_{30}$, so the power efficiency of the laser cannot exceed

$$\eta_{\text{atomic}} = \frac{\nu_{21}}{\nu_{30}} \tag{7.1-1}$$

to which quantity we will refer as the "atomic quantum efficiency." The overall laser efficiency depends on the fraction of the total pump power that is effective in transferring atoms into level 3 and on the pumping quantum efficiency defined as the fraction of the atoms that once in 3, make a transition

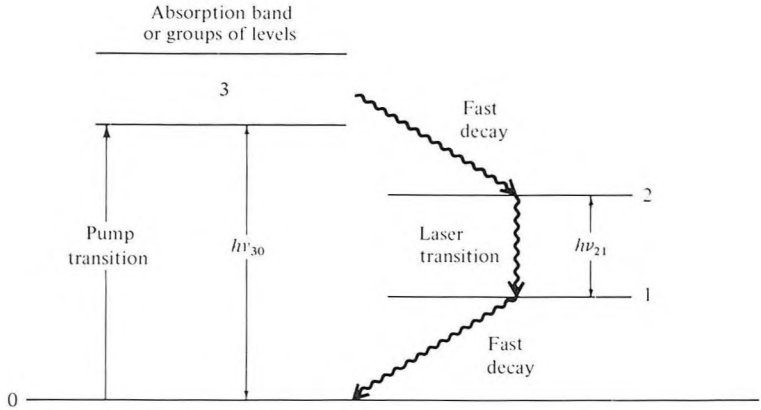

Figure 7-1 Pumping–oscillation cycle of a typical laser.

to 2. The product of the last two factors, which constitutes an upper limit on the efficiency of optically pumped lasers, ranges from about 1 percent for solid-state lasers such as Nd^{3+}:YAG, to about 30 percent in the CO_2 laser, and to near unity in the GaAs junction laser. We shall discuss these factors when we get down to some specific laser systems. We may note, however, that according to (7.1-1), in an efficient laser system ν_{21} and ν_{30} must be of the same order of magnitude, so the laser transition should involve low-lying levels.

7.2 RUBY LASER

The first material in which laser action was demonstrated [1] and still one of the most useful laser materials is ruby, whose output is at $\lambda_0 = 0.6943$ μm. The active laser particles are Cr^{3+} ions present as impurities in Al_2O_3 crystal. Typical Cr^{3+} concentrations are ~0.05 percent by weight. The pertinent energy level diagram is shown in Figure 7-2.

The pumping of ruby is usually performed by subjecting it to the light of intense flashlamps (quite similar to the types used in flash photography). A portion of this light that corresponds in frequency to the two absorption bands $^4F_2$ and $^4F_1$ is absorbed, thereby causing Cr^{3+} ions to be transferred into these levels. The ions proceed to decay, within an average time of $\omega_{32}^{-1} \simeq 5 \times 10^{-8}$ seconds [2], into the upper laser level ^2E. The level ^2E is composed of two separate levels $2\overline{A}$ and $\overline{E}$ separated by 29 cm^{-1}.[1] The lower of these two, $\overline{E}$, is the upper laser level. The lower laser level is the ground

[1]The unit 1 cm^{-1} (one wavenumber) is the frequency corresponding to $\lambda_0 = 1$ cm, so 1 cm^{-1} is equivalent to $\nu = 3 \times 10^{10}$ Hz. It is also used as a measure of energy where 1 cm^{-1} corresponds to the energy $h\nu$ of a photon with $\nu = 3 \times 10^{10}$ Hz.

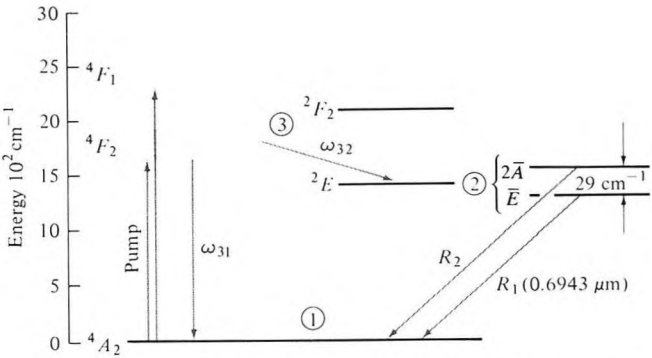

Figure 7-2 Energy levels pertinent to the operation of a ruby laser. (After Reference [2].)

state, and thus, according to the discussion of Section 6.3, ruby is a three-level laser. The lifetime of atoms in the upper laser level $\bar{E}$ is $t_2 \simeq 3 \times 10^{-3}$ second. Each decay results in the (spontaneous) emission of a photon, so $t_2 \simeq t_{\text{spont}}$.

An absorption spectrum of a typical ruby with two orientations of the optical field relative to the c (optic) axis is shown in Figure 7-3. The two main peaks correspond to absorption into the useful $^4F_1$ and $^4F_2$ bands, which are responsible for the characteristic (ruby) color.

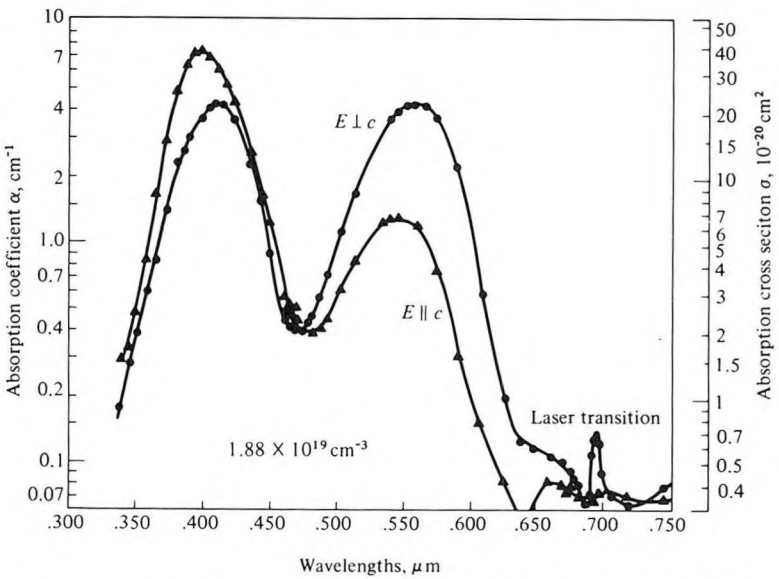

Figure 7-3 Absorption coefficient and absorption cross section as functions of wavelength for $E \| c$ and $E \perp c$. The 300 K data were derived from transmittance measurements on pink ruby with an average Cr ion concentration of 1.88×10^{19} cm^{-3}. (After Reference [3].)

The ordinate is labeled in terms of the absorption coefficient and in terms of the transition cross section σ, which may be defined as the absorption coefficient per unit inversion per unit volume and has consequently the dimension of area. According to this definition, $\alpha(\nu)$ is given by

$$\alpha(\nu) = (N_1 - N_2)\sigma(\nu) \tag{7.2-1}$$

A more detailed plot of the absorption near the laser emission wavelength is shown in Figure 7-4. The width $\Delta\nu$ of the laser transition as a function of temperature is shown in Figure 7-5. At room temperature, $\Delta\nu = 11\ \text{cm}^{-1}$.

We can use ruby to illustrate some of the considerations involved in optical pumping of solid-state lasers. Figure 7-6 shows a typical setup of an optically pumped laser, such as ruby. The helical flashlamp surrounds the ruby rod. The flash excitation is provided by the discharge of the charge stored in a capacitor bank across the lamp.

The typical flash output consists of a pulse of light of duration $t_{\text{flash}} \simeq 5 \times 10^{-4}$ seconds. Let us, for the sake of simplicity, assume that the flash pulse is rectangular in time and of duration t_{flash} and that it results in an optical flux at the crystal surface having $s(\nu)$ watts per unit area per unit frequency at the frequency ν. If the absorption coefficient of the crystal is $\alpha(\nu)$, then the amount of energy absorbed by the crystal per unit volume is[2]

$$t_{\text{flash}} \int_0^\infty s(\nu)\alpha(\nu)\, d\nu$$

[2]We assume that the total absorption in passing the crystal is small, so $s(\nu)$ is taken to be independent of the distance through the crystal.

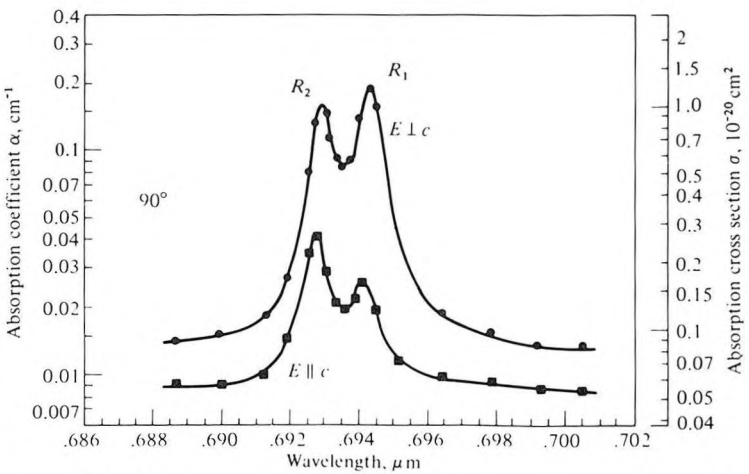

Figure 7-4 Absorption coefficient and absorption cross section as functions of wavelength for $E\|c$ and $E\perp c$. Sample was a pink ruby laser rod having a 90° c-axis orientation with respect to the rod axis and a Cr concentration of 1.58×10^{19} cm^{-3}. (After Reference [3].)

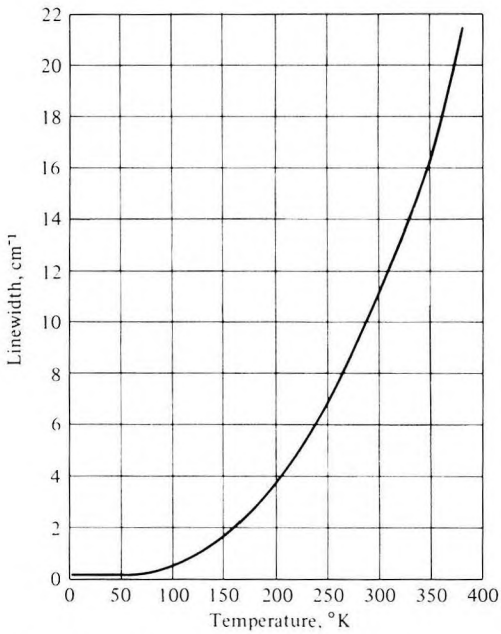

Figure 7-5 Linewidth of the R_1 line of ruby as a function of temperature. (After Reference [4].)

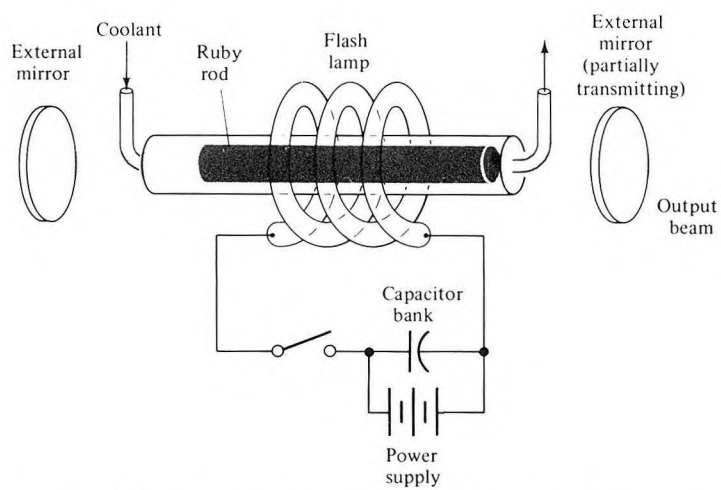

Figure 7-6 Typical setup of a pulsed ruby laser using flashlamp pumping and external mirrors.

If the absorption quantum efficiency (the probability that the absorption of a pump photon at ν results in transferring one atom into the upper laser level) is $\eta(\nu)$, the number of atoms pumped into level 2 per unit volume is

$$N_2 = t_{\text{flash}} \int_0^\infty \frac{s(\nu)\alpha(\nu)\eta(\nu)}{h\nu}\, d\nu \tag{7.2-2}$$

Since the lifetime $t_2 \simeq 3 \times 10^{-3}$ second of atoms in level 2 is considerably longer than the flash duration ($\sim 5 \times 10^{-4}$ s) we may neglect the spontaneous decay out of level 2 during the time of the flash pulse, so N_2 represents the population of level 2 after the flash.

Numerical Example: Flash Pumping of a Pulsed Ruby Laser

Consider the case of a ruby laser with the following parameters:

$$N_0 = 2 \times 10^{19} \text{ atoms/cm}^3 \ (\text{Cr}^{3+})$$
$$t_2 \simeq t_{\text{spont}} \simeq 3 \times 10^{-3} \text{ s}$$
$$t_{\text{flash}} = 5 \times 10^{-4} \text{ s}$$

If the useful absorption is limited to relatively narrow spectral regions, we may approximate (7.2-2) by

$$N_2 = \frac{t_{\text{flash}}\, \overline{s(\nu)}\, \overline{\alpha(\nu)}\, \overline{\eta(\nu)}\, \overline{\Delta\nu}}{h\bar{\nu}} \tag{7.2-3}$$

where the bars represent average values over the useful absorption region whose width is $\overline{\Delta\nu}$.

From Figure 7-3 we deduce an average absorption coefficient of $\overline{\alpha(\nu)} \simeq 2 \text{ cm}^{-1}$ over the two central peaks. Since ruby is a three-level laser, the upper level population is, according to (6.3-2), $N_2 \simeq N_0/2 = 10^{19} \text{ cm}^{-3}$. Using $\bar{\nu} \simeq 5 \times 10^{14}$ Hz, $\overline{\eta(\nu)} \simeq 1$ (7.2-3) yields

$$\bar{s}\, \overline{\Delta\nu} t_{\text{flash}} \simeq 1.5 \text{ J/cm}^2$$

for the pump energy in the useful absorption region that must fall on each square centimeter of crystal surface in order to obtain threshold inversion. To calculate the total lamp energy that is incident on the crystal we need to know the spectral characteristics of the lamp output. Typical data of this sort are shown in Figure 7-7. The mercury-discharge lamp is seen to contain considerable output in the useful absorption regions (near 4000 Å and 5500 Å) of ruby. If we estimate the useful fraction of the lamp output at 10 percent, the fraction of the lamp light actually incident on the crystal as 20 percent, and the conversion of electrical-to-optical energy as 50 percent, we find the threshold electric energy input to the flashlamp per square centimeter of

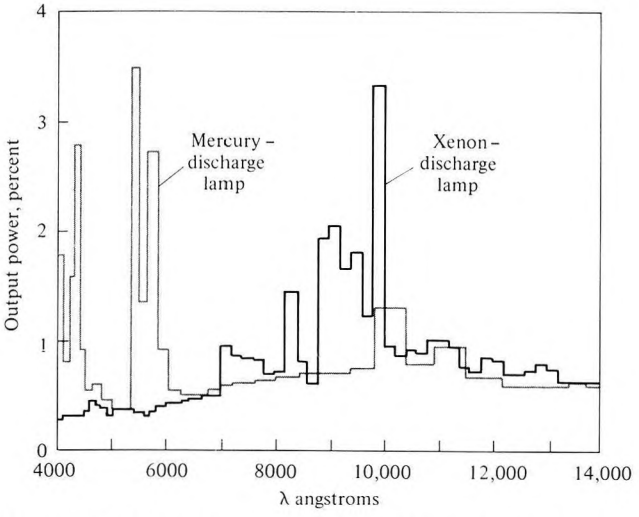

Figure 7-7 Spectral output characteristics of two commercial high-pressure lamps. Output is plotted as a fraction of electrical input to lamp over certain wavelength intervals (mostly 200 Å) between 0.4 and 1.4 μm. (After Reference [5].)

laser surface is

$$\frac{1.5}{0.1 \times 0.2 \times 0.5} = 150 \text{ J/cm}^2$$

These are, admittedly, extremely crude calculations. They are included not only to illustrate the order of magnitude numbers involved in laser pumping, but also as an example of the quick and rough estimates needed to discriminate between feasible ideas and "pie-in-the-sky" schemes.

7.3 Nd^{3+}:YAG LASER

One of the most important laser systems is that using trivalent neodymium ions (Nd^{3+}), which are present as impurities in yttrium aluminum garnet (YAG = $Y_3Al_5O_{12}$); see References [6, 7]. The laser emission occurs at $\lambda_0 = 1.0641$ μm at room temperature. The relevant energy levels are shown in Figure 7-8. The lower laser level is at $E_2 \simeq 2111$ cm^{-1} from the ground state so that at room temperature its population is down by a factor of $\exp(-E_2/kT) \simeq e^{-10}$ from that of the ground state and can be neglected. The Nd^{3+}:YAG thus fits our definition (see Section 6.3) of a four-level laser.

The spontaneous emission spectrum of the laser transition is shown in Figure 7-9. The width of the gain linewidth at room temperature is $\Delta\nu \simeq 6$ cm^{-1}. The spontaneous lifetime for the laser transition has been

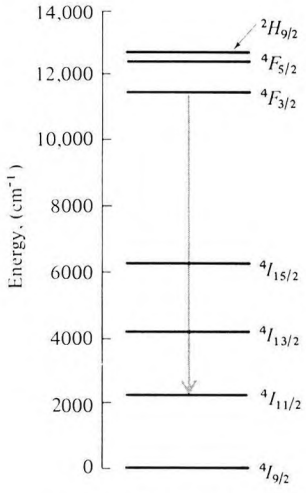

Figure 7-8 Energy-level diagram of Nd^{3+} in YAG. (After Reference [6].)

measured [7] as $t_{spont} = 5.5 \times 10^{-4}$ s. The room-temperature cross section at the center of the laser transition is $\sigma = 9 \times 10^{-19}$ cm^2. If we compare this number to $\sigma = 1.22 \times 10^{-20}$ cm^2 in ruby (see Figure 7-4), we expect that at a given inversion the optical gain constant γ in Nd^{3+}:YAG is approximately 75 times that of ruby. This causes the oscillation threshold to be very low and explains the easy continuous (CW) operation of this laser compared to ruby.

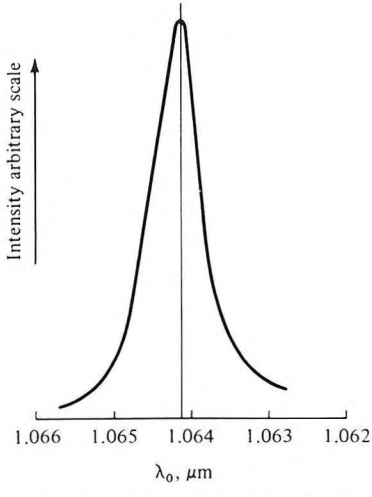

Figure 7-9 Spontaneous-emission spectrum of Nd^{3+} in YAG near the laser transition at $\lambda_0 = 1.064$ μm. (After Reference [7].)

The absorption responsible for populating the upper laser level takes place in a number of bands between 13,000 and 25,000 cm^{-1}.

Numerical Example: Threshold of an Nd^{3+}:YAG Laser

Pulsed threshold First we estimate the energy needed to excite a typical Nd^{3+}:YAG laser on a pulse basis so that we can compare it with that of ruby. We use the following data:

$$\left.\begin{aligned} l &= 20 \text{ cm (length optical resonator)} \\ L &= 4 \text{ percent (= loss per pass)} \\ n &= 1.5 \end{aligned}\right\} t_c = \frac{nl}{Lc} = 2.5 \times 10^{-8} \text{ s}$$

$$\Delta\nu = 6 \text{ cm}^{-1} (= 6 \times 3 \times 10^{10} \text{ Hz})$$

$$t_{\text{spont}} = 5.5 \times 10^{-4} \text{ s}$$

$$\lambda = 1.06 \ \mu\text{m}$$

Using the foregoing data in (6.1-11) gives

$$N_t = \frac{8\pi n^3 t_{\text{spont}} \, \Delta\nu}{c t_c \lambda^2} \simeq 1.0 \times 10^{15} \text{ cm}^{-3}$$

Assuming that 5 percent of the exciting light energy falls within the useful absorption bands, that 5 percent of this light is actually absorbed by the crystal, that the average ratio of laser frequency to the pump frequency is 0.5, and that the lamp efficiency (optical output/electrical input) is 0.5, we obtain

$$\mathscr{E}_{\text{lamp}} = \frac{N_t h\nu_{\text{laser}}}{5 \times 10^{-2} \times 5 \times 10^{-2} \times 0.5 \times 0.5} \simeq 0.3 \text{ J/cm}^3$$

for the energy input to the lamp at threshold.

It is interesting to compare this last number to the figure of 150 joules per square centimeter of surface area obtained in the ruby example of Section 7.2. For reasonable dimension crystals (say, length = 5 cm, r = 2 mm) we obtain $\mathscr{E}_{\text{lamp}} = 0.19$ J. We expect the ruby threshold to exceed that of Nd^{3+}:YAG by three orders of magnitude, which is indeed the case.

Continuous operation The critical fluorescence power—that is, the actual power given off by spontaneous emission just below threshold—is given by (6.3-4) as

$$\left(\frac{P_s}{V}\right) = \frac{N_t h\nu}{t_{\text{spont}}} \simeq 0.34 \text{ W/cm}^3$$

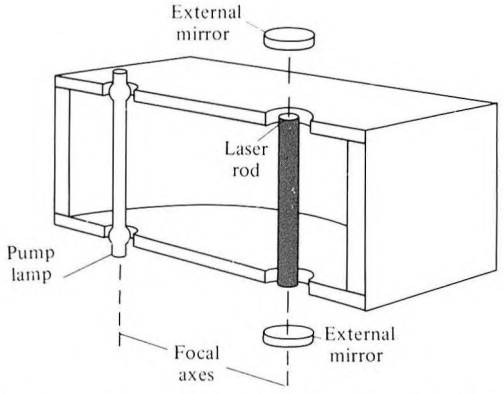

Figure 7-10 Typical continuous solid-state laser arrangement employing an elliptic cylinder housing for concentrating lamp light onto laser.

Taking the crystal diameter as 0.25 cm and its length as 3 cm and using the same efficiency factors assumed in the first part of this example, we can estimate the power input to the lamp at threshold as

$$P_{(\text{to lamp})} = \frac{0.34 \times (\pi/4) \times (0.25)^2 \times 3}{5 \times 10^{-2} \times 5 \times 10^{-2} \times 0.5 \times 0.5} \simeq 81 \text{ watts}$$

which is in reasonable agreement with experimental values [6].

A typical arrangement used in continuous solid state lasers is shown in Figure 7-10. The highly polished elliptic cylinder is used to concentrate the light from the lamp, which is placed along one focal axis, onto the laser rod, which occupies the other axis. This configuration guarantees that most of the light emitted by the lamp passes through the laser rod. The reflecting mirrors are placed outside the cylinder.

7.4 NEODYMIUM-GLASS LASER

One of the most useful laser systems is that which results when the Nd^{3+} ion is present as an impurity atom in glass [8].

The energy levels involved in the laser transition in a typical glass are shown in Figure 7-11. The laser emission wavelength is at $\lambda = 1.059\ \mu m$ and the lower level is approximately 1950 cm^{-1} above the ground state. As in the case of Nd^{3+}:YAG described in Section 7.3, we have here a four-level laser, since the thermal population of the lower laser level is negligible. The fluorescent emission near $\lambda_0 = 1.06\ \mu m$ is shown in Figure 7-12. The fluorescent linewidth can be measured off directly and ranges, for the glasses shown, around 300 cm^{-1}. This width is approximately a factor of 50 larger

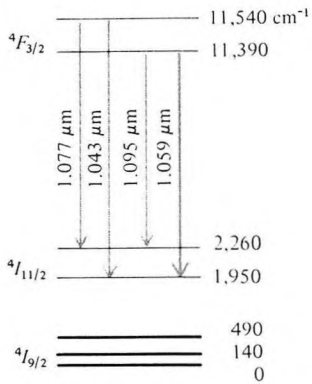

Figure 7-11 Energy-level diagram for the ground state and the states involved in laser emission at 1.059 μm for Nd^{3+} in a rubidium potassium barium silicate glass. (After Reference [8].)

than that of Nd^{3+} in YAG. This is due to the amorphous structure of glass, which causes different Nd^{3+} ions to "see" slightly different surroundings. This causes their energy splittings to vary slightly. Different ions consequently radiate at slightly different frequencies, causing a broadening of the spontaneous emission spectrum. The absorption bands responsible for pumping the laser level are shown in Figure 7-13. The probability that the absorption of a photon in any of these bands will result in pumping an atom to the upper laser level (that is, the absorption quantum efficiency) has been estimated [8] at about 0.4.

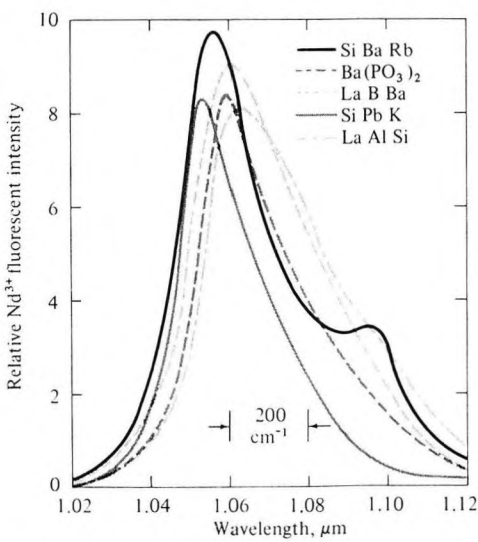

Figure 7-12 Fluorescent emission of the 1.06-μm line of Nd^{3+} at 300 K in various glass bases. (After Reference [8].)

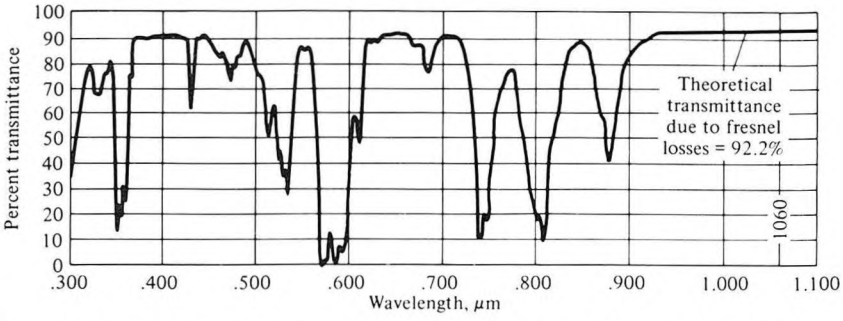

Figure 7-13 Nd^{3+} absorption spectrum for a sample of glass 6.4 mm thick with the composition 66 wt.% SiO_2, 5 wt.% Nd_2O_3, 16 wt.% Na_2O, 5 wt.% BaO, 2 wt.% Al_2O_3, and 1 wt.% Sb_2O_3. (After Reference [8].)

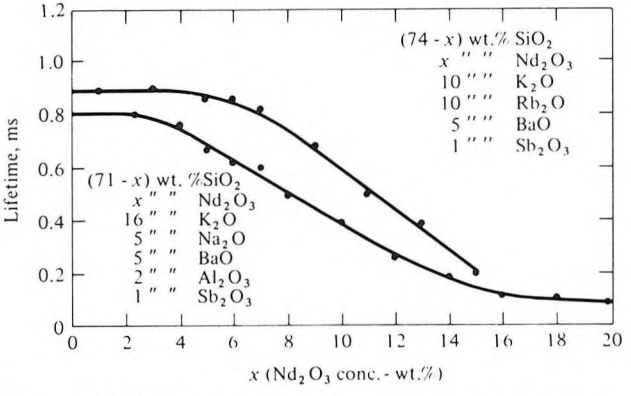

Figure 7-14 Lifetime as a function of concentration for two glass series. (After Reference [8].)

The lifetime t_2 of the upper laser level depends on the host glass and on the Nd^{3+} concentration. This variation in two glass series is shown in Figure 7-14.

Numerical Example: Thresholds for CW and Pulsed Operation of Nd^{3+}:Glass Lasers

Let us estimate first the threshold for continuous (CW) laser action in a Nd^{3+} glass laser using the following data:

$$\Delta\nu = 200 \text{ cm}^{-1} \qquad \text{(see Figure 7-12)}$$

$$n = 1.5$$

$$t_{\text{spont}} \simeq t_2 = 3 \times 10^{-4} \text{ s}$$

$$\left.\begin{aligned} l &= \text{length of resonator} = 20 \text{ cm} \\ L &= \text{loss per pass} = 2 \text{ percent} \end{aligned}\right\} t_c \simeq \frac{nl}{Lc} = 5 \times 10^{-8} \text{ s}$$

Using (6.1-11) we obtain

$$N_t = \frac{8\pi t_{\text{spont}} n^3 \Delta\nu}{c t_c \lambda^2} = 9.05 \times 10^{15} \text{ atoms/cm}^3$$

for the critical inversion. The fluorescence power at threshold P_s is thus [see (6.3-5)]

$$P_s = \frac{N_t h\nu V}{t_{\text{spont}}} = 5.65 \text{ watts}$$

in a crystal volume $V = 1 \text{ cm}^3$.

We assume (a) that only 10 percent of the pump light lies within the useful absorption bands, (b) that because of the optical coupling inefficiency and the relative transparency of the crystal only 10 percent of the energy leaving the lamp within the absorption bands is actually absorbed, (c) that the absorption quantum efficiency is 40 percent, and (d) that the average pumping frequency is twice that of the emitted radiation. The lamp output at threshold is thus

$$\frac{2 \times 5.65}{0.1 \times 0.1 \times 0.4} = 2825 \text{ watts}$$

If the efficiency of the lamp in converting electrical to optical energy is about 50 percent, we find that continuous operation of the laser requires about 5 kW of power. This number is to be contrasted with a threshold of approximately 100 watts for the Nd:YAG laser, which helps explain why Nd:glass lasers are not operated continuously.

If we consider the pulsed operation of a Nd:glass laser by flash excitation, we have to estimate the minimum energy needed to pump the laser at threshold. Let us assume here that the losses (attributable mostly to the output mirror transmittance) are $L = 20$ percent.[3] A recalculation of N_t gives

$$N_t = 9.05 \times 10^{16} \text{ atoms/cm}^3$$

The minimum energy needed to pump N_t atoms into level 2 is then

$$\frac{\mathscr{E}_{\min}}{V} = N_t(h\nu) = 1.7 \times 10^{-2} \text{ J/cm}^3$$

Assuming a crystal volume $V = 10 \text{ cm}^3$ and the same efficiency factors used in the CW example above, we find that the input energy to the flashlamp at

[3]Because of the higher pumping rate available with flash pumping, optimum coupling (see Section 6.5) calls for larger mirror transmittances compared to the CW case.

threshold $\simeq 2 \times 1.7 \times 10^{-2} \times 10/(0.1 \times 0.1 \times 0.4) = 85$ J. Typical Nd^{3+}:glass lasers with characteristics similar to those used in this example are found to require an input of about 150–300 joules at threshold.

7.5 He–Ne LASER

The first CW laser, as well as the first gas laser, was one in which a transition between the $2S$ and the $2p$ levels in atomic Ne resulted in the emission of 1.15 μm radiation [9]. Since then transitions in Ne were used to obtain laser oscillation at $\lambda_0 = 0.6328$ μm [10] and at $\lambda_0 = 3.39$ μm. The operation of this laser can be explained with the aid of Figure 7-15. A dc (or rf) discharge is established in the gas mixture containing typically, 1.0 mm Hg of He and 0.1 mm of Ne. The energetic electrons in the discharge excite helium atoms into a variety of excited states. In the normal cascade of these excited atoms down to the ground state, many collect in the long-lived metastable states

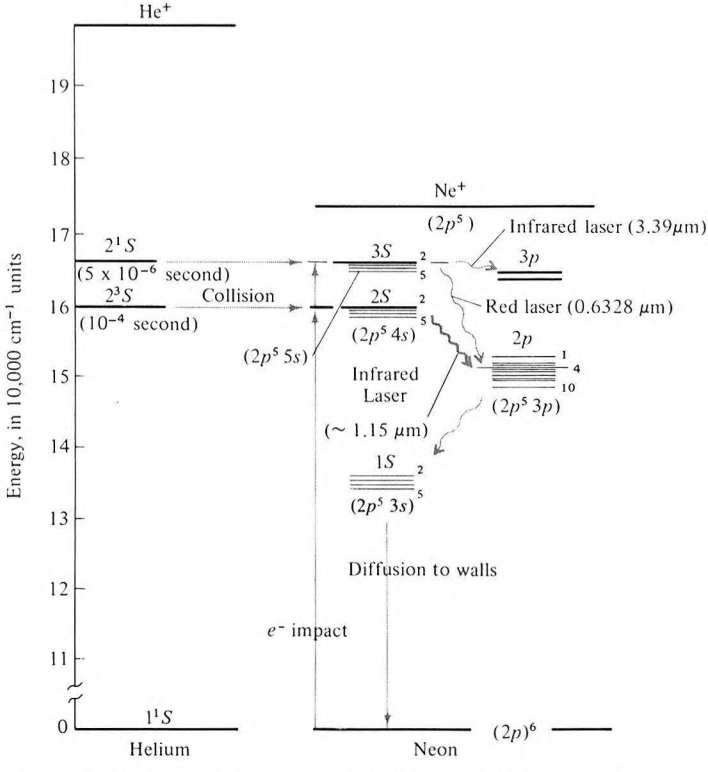

Figure 7-15 He–Ne energy levels. The dominant excitation paths for the red and infrared laser–maser transitions are shown. (After Reference [11].)

2^3S and 2^1S whose lifetimes are 10^{-4} second and 5×10^{-6} second, respectively. Since these long-lived (metastable) levels nearly coincide in energy with the $2S$ and $3S$ levels of Ne, they can excite Ne atoms into these two excited states. This excitation takes place when an excited He atom collides with a Ne atom in the ground state and exchanges energy with it. The small difference in energy ($\sim$400 cm^{-1} in the case of the $2S$ level) is taken up by the kinetic energy of the atoms after the collision. This is the main pumping mechanism in the He–Ne system.

1. *The 0.6328 μm oscillation.* The upper level is one of the Ne $3S$ levels, whereas the terminal level belongs to the $2p$ group. The terminal ($2p$) level decays radiatively with a time constant of about 10^{-8} second into the long-lived $1S$ state. This time is much shorter than the 10^{-7} second lifetime of the upper laser level $3S$. The condition $t_1 < t_2$ for population inversion in the $3S$-$2p$ transition (see Section 6.4) is thus fulfilled.

   Another important point involves the level $1S$. Because of its long life it tends to collect atoms reaching it by radiative decay from the lower laser level $2p$. Atoms in $1S$ collide with discharge electrons and are excited back into the lower laser level $2p$. This reduces the inversion. Atoms in the $1S$ states relax back to the ground state mostly in collisions with the wall of the discharge tube. For this reason the gain in the 0.6328 μm transition is found to increase with decreasing tube diameter.
2. *The 1.15 μm oscillation.* The upper laser level $2S$ is pumped by resonant (that is, energy-conserving) collisions with the metastable 2^3S He level. It uses the same lower level as the 0.6328 μm transition and, consequently, also depends on wall collisions to depopulate the $1S$ Ne level.
3. *The 3.39 μm oscillation.* This involves a $3S$–$3p$ transition and thus uses the same upper level as the 0.6328 μm oscillation. It is remarkable for the fact that it provides a small-signal optical gain of about 50 dB/m.[4] This large gain reflects partly the inverse dependence of γ on ν^2 [see Equation (5.3-3)] as well as the short lifetime of the $3p$ level, which allows the buildup of a large inversion.

   Because of the high gain in this transition, oscillation would normally occur at 3.39 μm rather than at 0.6328 μm. The reason is that the threshold condition will be reached first at 3.39 μm and, once that happens, the gain "clamping" will prevent any further buildup of the population of $3S$. The 0.6328 μm lasers overcome this problem by introducing into the optical path elements, such as glass or quartz Brewster windows, that absorb strongly at 3.39 μm but not at 0.6328 μm. This raises the threshold pumping level for the 3.39 μm oscillation above that of the 0.6328 μm oscillation.

[4]This is not the actual gain that exists inside the laser resonator, but the one-pass gain exercised by a very small input wave propagating through the discharge. In the laser the gain per pass is reduced by saturation until it equals the loss per pass.

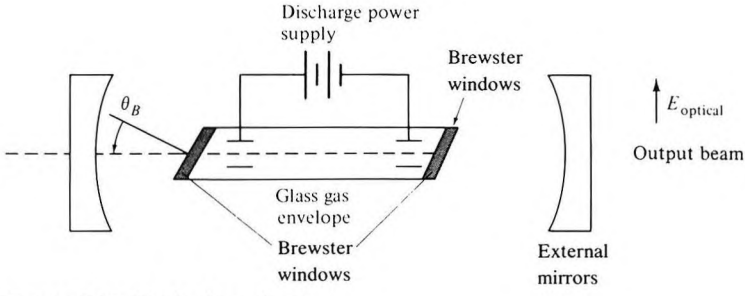

Figure 7-16 Typical gas laser.

A typical gas laser setup is illustrated by Figure 7-16. The gas envelope windows are tilted at Brewster's angle θ_B, so radiation with the electric field vector in the plane of the paper suffers no reflection losses at the windows. This causes the output radiation to be polarized in the sense shown, since the orthogonal polarization (the E vector out of the plane of the paper) undergoes reflection losses at the windows and, consequently, has a higher threshold.

7.6 CARBON DIOXIDE LASER

The lasers described so far in this chapter depend on electronic transitions between states in which the electronic orbitals (that is, charge distributions around the atomic nucleus) are different. As an example, consider the red (0.6328 μm) transition in Ne shown in Figure 7-15. It involves levels $2p^5 5s$ and $2p^5 3p$ so that in making a transition from the upper to the lower laser level one of the six outer electrons changes from a hydrogen-like state $5s$ (that is, $n = 5$, $l = 0$) to one in which $n = 3$ and $l = 1$.

The CO_2 laser [12] is representative of the so-called molecular lasers in which the energy levels of concern involve the internal vibration of the molecules—that is, the relative motion of the constituent atoms. The atomic electrons remain in their lowest energetic states and their degree of excitation is not affected.

As an illustration, consider the simple case of the nitrogen molecule. The molecular vibration involves the relative motion of the two atoms with respect to each other. This vibration takes place at a characteristic frequency of $\nu_0 = 2326\ \text{cm}^{-1}$, which depends on the molecular mass as well as the elastic restoring force between the atoms [13]. According to basic quantum mechanics, the degrees of vibrational excitation are discrete (that is, quantized) and the energy of the molecule can take on the values $h\nu_0(v + \frac{1}{2})$, where $v = 0, 1, 2, 3, \ldots$. The energy-level diagram of N_2 (in its lowest electronic state) would then ideally consist of an equally spaced set of levels with a spacing of $h\nu_0$. The ground state ($v = 0$) and the first excited state ($v = 1$) are shown on the right side of Figure 7-17.

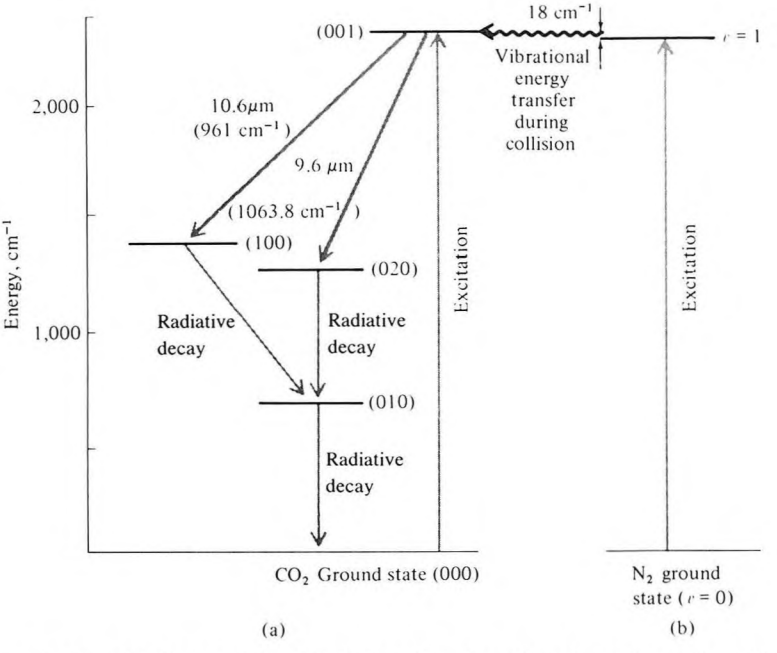

Figure 7-17 (a) Some of the low-lying vibrational levels of the carbon dioxide (CO_2) molecule, including the upper and lower levels for the 10.6 μm and 9.6 μm laser transitions. (b) Ground state ($v = 0$) and first excited state ($v = 1$) of the nitrogen molecule, which plays an important role in the selective excitation of the (001) CO_2 level.

The CO_2 molecule presents a more complicated case. Since it consists of three atoms, it can execute three basic internal vibrations, the so-called normal modes of vibration. These are shown in Figure 7-18. In (a) the molecule is at rest. In (b) the atoms vibrate along the internuclear axis in a symmetric manner. In (c) the molecules vibrate symmetrically along an axis perpendicular to the internuclear axis—the bending mode. In (d) the atoms vibrate asymmetrically along the internuclear axis. The mode is referred to as the asymmetric stretching mode. In the first approximation one can assume that the three normal modes are independent of each other, so the state of the CO_2 molecule can be described by a set of three integers (v_1, v_2, v_3) that correspond respectively to the degree of excitation of the three modes described. The total energy of the molecule is thus

$$E(v_1, v_2, v_3) = h\nu_1(v_1 + \tfrac{1}{2}) + h\nu_2(v_2 + \tfrac{1}{2}) + h\nu_3(v_3 + \tfrac{1}{2}) \qquad (7.6\text{-}1)$$

where ν_1, ν_2, ν_3 are the frequencies of the symmetric stretch, bending, and asymmetric stretch modes, respectively.

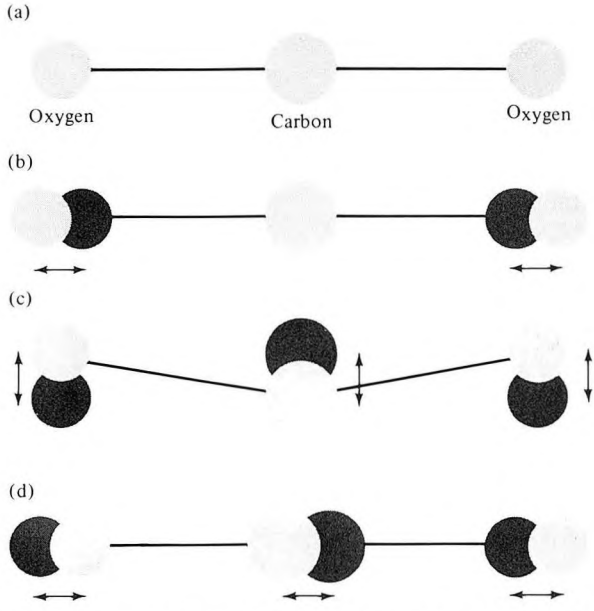

Figure 7-18 (a) Unexcited CO_2 molecule. (b), (c), and (d) The three normal modes of vibration of the CO_2 molecule. (After Reference [14].)

Some of the low vibrational levels of CO_2 are shown in Figure 7-17. The upper laser level (001) is thus one in which only the asymmetric stretch mode, Figure 7-18(d), is excited and contains a single quantum $h\nu_3$ of energy.

The laser transition at 10.6 μm takes place between the (001) and (100) levels of CO_2. The excitation is provided usually in a plasma discharge that, in addition to CO_2, typically contains N_2 and He. The CO_2 laser possesses a high overall working efficiency of about 30 percent. This efficiency results primarily from three factors: (a) The laser levels are all near the ground state, and the atomic quantum efficiency ν_{21}/ν_{30}, which was discussed in Section 7.1, is about 45 percent; (b) a large fraction of the CO_2 molecules excited by electron impact cascade down the energy ladder from their original level of excitation and tend to collect in the long-lived (001) level; (c) a very large fraction of the N_2 molecules that are excited by the discharge tend to collect in the $v = 1$ level. Collisions with ground-state CO_2 molecules result in transferring their excitation to the latter, thereby exciting them to the (001) state as shown in Figure 7-17. The slight deficiency in energy (about 18 cm^{-1}) is made up by a decrease of the total kinetic energy of the molecules following the collision. This collision can be represented by

$$(v = 1) + (000) + \text{K.E.} = (v = 0) + (001) \qquad (7.6\text{-}2)$$

and has a sufficiently high cross section that at the pressures and temper-

atures involved in the operation of a CO_2 laser most of the N_2 molecules in the $v = 1$ lose their excitation energy by this process.[5]

Carbon dioxide lasers are not only efficient but can emit large amounts of power. Laboratory-size lasers with discharge envelopes of a few feet in length can yield an output of a few kilowatts. This is due not only to the very *selective* excitation of the low-lying upper laser level, but also to the fact that once a molecule is stimulated to emit a photon it returns quickly to the ground state, where it can be used again. This is accomplished mostly through collisions with other molecules—such as that of He, which is added to the gas mixture.

7.7 Ar^+ LASER

Transitions between highly excited states of the singly ionized argon atom can be used to obtain oscillation at a number of visible (or near visible) wavelengths between 0.35 and 0.52 μm; see References [15, 16]. The Ar^+ laser is consequently one of the most important lasers in use today. The pertinent energy level scheme is shown in Figure 7-19. The most prominent transition is the one at 4880 Å.

The Ar^+ laser can be operated in a pure Ar discharge that contains no other gases. The excitation mechanism involves collisions with energetic (~4–5 eV) electrons. Since the mean electron energy is small compared to the energy of the upper laser level (~20 eV above the ground state of the ion), it is clear that pumping is achieved by multiple collisions of Ar^+ ground-state ions with electrons followed by a number of cascading paths. The details of the collision and cascading processes are not clearly understood.

7.8 EXCIMER LASERS

The term *excimer* was introduced originally [17, 20] to describe a homopolar dimer such as Xe_2 or Hg_2 that is bound (i.e., the atoms are attracted to each other thus forming a stable molecule) in an excited state, but which dissociates in its ground state. The term *exciplex* was used to describe heteropolar cases such as XeF, where the constituent atoms are different.

The distinction between the two terms has been lost to a large extent, and bowing to popular usage we will refer to exciplex molecules as excimers.

The interest in excimer lasers principally of heavy noble gases (Xe, Kr, Ar) and the halogens (F, Cl, Br, I) is due to the relatively efficient production

---

[5]The cross section σ was defined in Section 7.2. In the present context it follows directly from the definition that the number of collisions of the type described by (7.6-2) per unit volume per unit time is equal to $N(v = 1)N(000)\sigma\bar{v}$ where $N(v = 1)$ and $N(000)$ are the densities of molecules in the states $v = 1$ of N_2 and (000) of CO_2, respectively. $\bar{v}$ is the (mean) relative velocity of the colliding molecules.

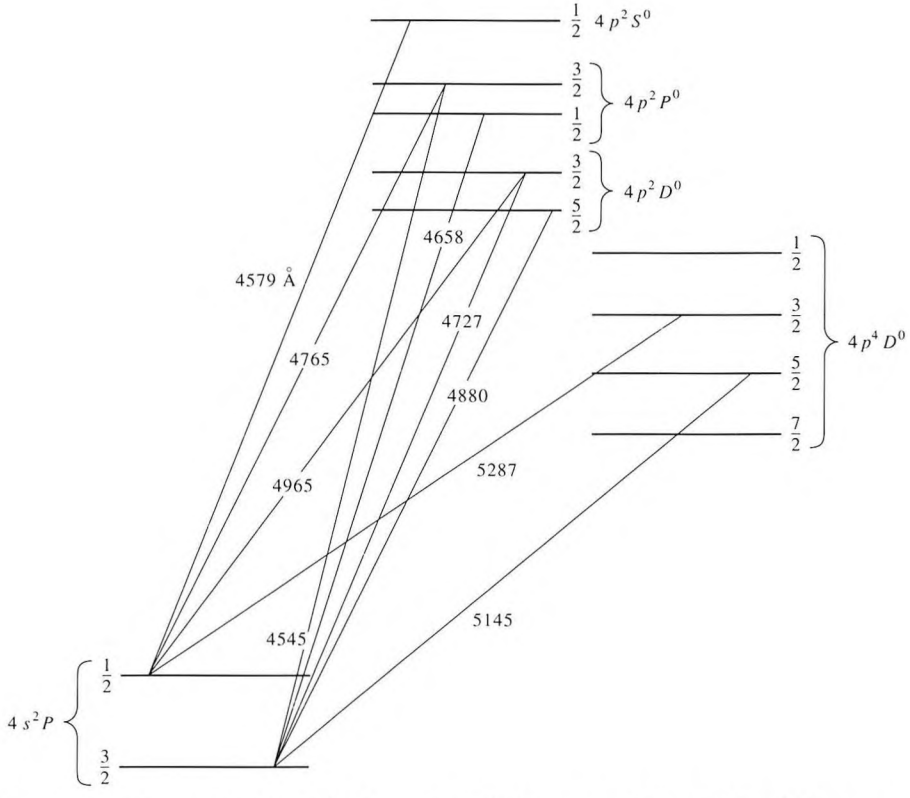

Figure 7-19 Energy levels of the $4p \rightarrow 4s$ Ar II laser transitions. (After Reference [15] with a correction supplied by the author.)

of their excited state by electron beam collisions and the fact that their emission wavelengths lie in the ultraviolet and vacuum ultraviolet ($0.2 < \lambda < 0.4$ μm) region of the spectrum, a region not covered well by other types of lasers. In what follows, we will limit our discussion to the noble gas halide lasers [20] which have, to date, yielded the best laser performance.

When the ionization energy (energy to remove an electron from the outermost shell) of an atom A is less than the sum of the electron affinity (energy released during electron attachment) of X, plus the electrostatic attraction energy between A^+ and X^-, the process of forming the ionic molecule (A^+X^-) via the process ($A + X$) $\rightarrow$ (A^+X^-) is exothermic (energy is released) and is favored. In the case of KrF, for example, this is when Kr is in an excited state (Kr*), since the ionization energy of Kr* is less than that of Kr. The ionization energies of Ar and Kr, as an example, are 15.68 and 13.93 eV, respectively, while in the excited state it is ~5 eV. The electron affinity of Cl is ~3.75 eV, while the repulsive energy is ~1 eV. The Coulomb attraction is ~8 eV. It follows that the process of forming KrCl

(starting with Kr and Cl in their ground state) is endothermic and requires the investment of ~4 eV per molecule, while if we start with excited Kr (Kr*) the process is exothermic and releases some 6 eV per molecule. To summarize:

$$A + X \longrightarrow (A^+X^-) - 4\text{ eV}$$
$$A^* + X \longrightarrow (A^+X^-)^* + 6\text{ eV}$$

Typical generalized potential curves for an excimer molecule AX in its excited state (AX)* and ground state AX are shown in Figure 7-20.

The lifetime of the upper bound state in KrF is ~6–10 ns, while that of the lower (repulsive) state is $\sim 10^{-13}$ s. This results in broad spontaneous emission with typical widths of 200–400 cm^{-1}. The emission wavelength of a laser that uses the excimer as the gain medium can be tuned over most of the region spanned by the spontaneous emission.

The noble gas lasers offer the possibility of generating and amplifying the pulses (2–8 ns) to very high (~50 kJ) energies. The lasers are relatively efficient when pumped by energetic electron beams (e-beam). High-current (1–10 kA) high-voltage (0.25–2 MeV) beams are utilized. A typical e-beam excited KrF excimer laser configuration is shown in Figure 7-21. The basic kinetics of the $Ar/Kr/F_2$ gas mixture used in KrF has been elucidated by Rokni et al. [18]. The main effect of the pumping e-beam is to form Kr_2^+ and F^-. This is followed by the ionic recombination reaction [19]

$$Kr_2^+ + F^- + Ar \longrightarrow (KrF)^* + Kr + Ar$$

The excited molecules KrF* thus form the inverted population gain medium.

Due to the shortness of the excited state lifetime ($\sim 6-8 \times 10^{-9}$ s), the excimer laser is used mostly for amplifying short pulses. In a gas mixture of 93.5% Ar, 6% Kr, and 0.3% F_2 with a total pressure of 1 atm excited by

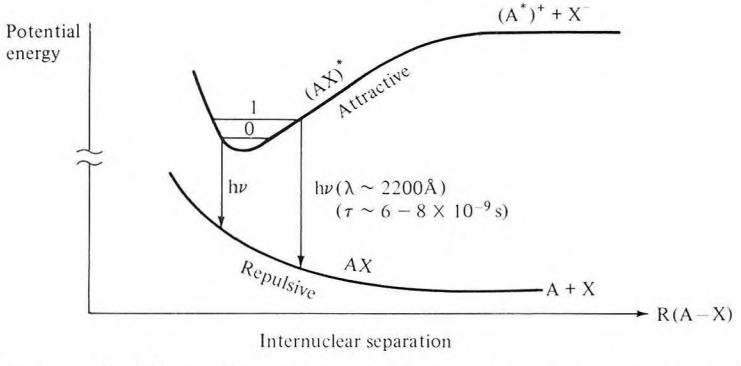

Figure 7-20 Potential energy curves for the ground state and an excited state of a typical nobel gas (A)–halide (X) molecule. The excited state is bound (i.e., possesses a minimum), while the ground state is repulsive. The two lowest vibrational states of the excimer state (AX)* are shown.

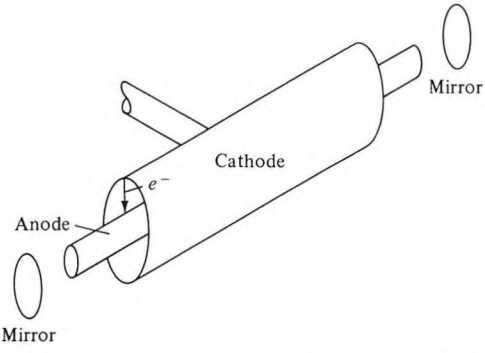

Figure 7-21 An excimer laser with a coaxial e-beam exciting geometry. (After Reference [20].)

a high-energy electron beam, as much as 30 percent of the pumping beam energy results in the production of KrF* excited-state molecules. Total amplified output of ~100 kJ and overall wall plug to optical output amplifier efficiencies of ~8 percent appear feasible [19]. This is the main interest for the current high level of activity in this laser system.

7.9 ORGANIC-DYE LASERS

Many organic dyes (that is, organic compounds that absorb strongly in certain visible-wavelength regions) also exhibit efficient luminescence, which often spans a large wavelength region in the visible portion of the spectrum. This last property makes it possible to obtain an appreciable tuning range from dye lasers; see References [21–30].

A schematic representation of an organic dye molecule (such as rhodamine 6G, for example) is shown in Figure 7-22.

State S_0 is the ground state. S_1, S_2, T_1, and T_2 are excited electronic states—that is, states in which one ground-state electron is elevated to an excited orbit. Typical energy separation, such as S_0–S_1 is about 20,000 cm^{-1}. In a singlet (S) state, the magnetic spin of the excited electron is antiparallel to the spin of the remaining molecule. In a triplet (T) state, the spins are parallel. Singlet → triplet, or triplet → singlet transitions thus involve a spin flip and are far less likely than transitions between two singlet or between two triplet states.

Transitions between two singlet states or between two triplet states, which are spin-allowed (that is, they do not involve a spin flip), give rise to intense absorption and fluorescence. The characteristic color of organic dyes is due to the $S_0 \rightarrow S_1$ absorption.

The singlet and triplet states, in turn, are split further into vibrational levels shown as heavy horizontal lines in Figure 7-22. These correspond to

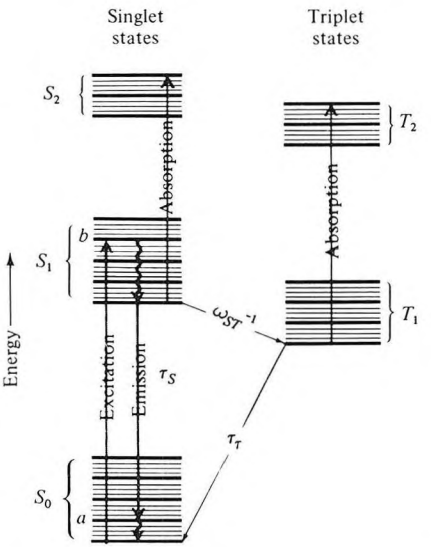

Figure 7-22 Schematic representation of the energy levels of an organic dye molecule. The heavy horizontal lines represent vibrational states and the lighter lines represent the rotational fine structure. Excitation and laser emission are represented by the transitions $A \rightarrow b$ and $B \rightarrow a$, respectively.

the quantized vibrational states of the organic molecule, as discussed in detail in Section 7.6. Typical energy separation between two adjacent vibrational levels within a given singlet or triplet state is about 1500 cm^{-1}. The fine splitting shown corresponds to rotational levels whose spacing is about 15 cm^{-1}.[6]

In the process of pumping the laser, the molecule is first excited, by absorbing a pump photon, into a rotational–vibrational state b within S_1. This is followed by a very fast decay to the bottom of the S_1 group, with the excess energy taken up by the vibrational and rotational energy of the molecules. Most of the excited molecules will then decay spontaneously to state a, emitting a photon of energy $\nu = (E_B - E_a)/h$. The lifetime for this process is τ_S.

There is, however, a small probability, approximately $\omega_{ST}\tau_S$, that an excited molecule will decay instead to the triplet state T_1, where ω_{ST} is the rate per molecule for undergoing an $S_1 \rightarrow T_1$ transition. Since this is a spin-forbidden transition, its rate is usually much smaller than the spontaneous decay rate τ_S^{-1}, so that $\omega_{ST}\tau_S \ll 1$. The lifetime τ_T for decay of T_1 to the ground state is relatively long (since this too is a spin-forbidden transition) and may vary from 10^{-7} to 10^{-3} second, depending on the experimental

[6] A transition between two adjacent rotational levels involves a change in the total angular momentum of the molecule about some axis.

conditions [24]. Owing to its relatively long lifetime, the triplet state T_1 acts as a trap for excited molecules. The absorption of molecules due to a $T_1 \rightarrow T_2$ transition is spin-allowed and is therefore very strong. If the wavelength region of this absorption coincides with that of the laser emission [at $\nu \simeq (E_B - E_a)/h$], an accumulation of molecules in T_1 increases the laser losses and at some critical value quenches the laser oscillation. For this reason, many organic-dye lasers operate only on a pulsed basis. In these cases fast-rise-time pump pulses—often derived from another laser [22]—cause a buildup of the S_1 population with oscillation taking place until an appreciable buildup of the T_1 population occurs.

Another basic property of molecules is that the peak of the absorption spectrum usually occurs at shorter wavelengths than the peak of the corresponding emission spectrum. This is illustrated in Figure 7-23, which shows the absorption and emission spectra of rhodamine 6G, which when dissolved in H_2O is used as a CW laser medium [26]. Laser oscillation occurring near the peak of the emission curve is thus absorbed weakly. But for this fortunate circumstance, laser action involving electronic transitions in molecules would not be possible.

Typical excitation and oscillation waveforms of a dye laser are shown in Figure 7-24. The possibility of quenching the laser action by triplet state absorption is evident.

A list of some common laser dyes is given in Table 7-1.

The broad fluorescence spectrum of the organic dyes suggests a broad tunability range for lasers using them as the active material. The spectrum

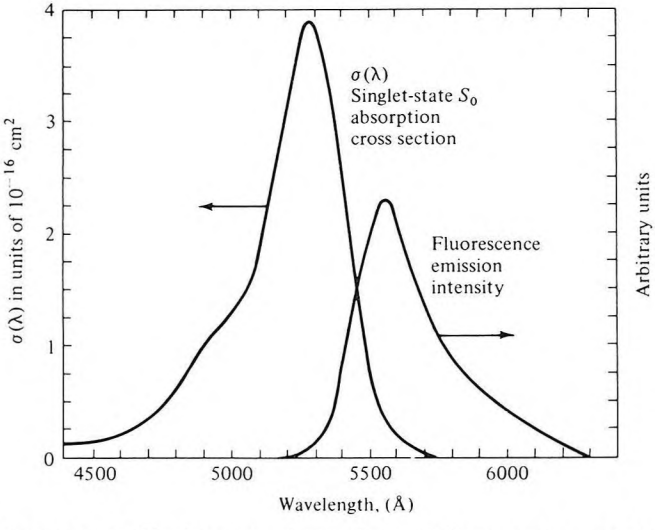

Figure 7-23 Singlet-state absorption and fluorescence spectra of rhodamine 6G obtained from measurements with a 10^{-4} molar ethanol solution of the dye. (After Reference [24].)

Table 7-1 Molecular Structure, Laser Wavelength, and Solvents for Some Laser Dyes (After Reference [24].)

Dye	Structure	Solvent	Wavelength
Acridine red	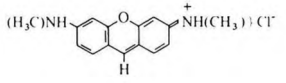	EtOH	Red 600–630 nm
Puronin B	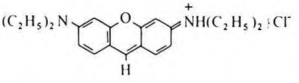	MeOH H_2O	Yellow
Rhodamine 6G	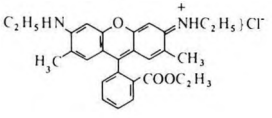	EtOH MeOH H_2O DMSO Polymethyl-methacrylate	Yellow 570–610 nm
Rhodamine B	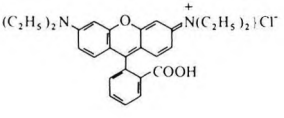	EtOH MeOH Polymethyl-methacrylate	Red 605–635 nm
Na-fluorescein	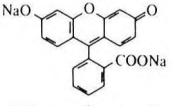	EtOH H_2O	Green 530–560 nm
2,7-Dichloro-fluorescein	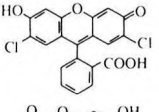	EtOH	Green 530–560 nm
7-Hydroxycoumarin	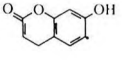	H_2O (pH ~ 9)	Blue 450–470 nm
4-Methylumbelli-ferone	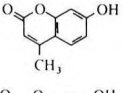	H_2O (pH ~ 9)	Blue 450–470 nm
Esculin	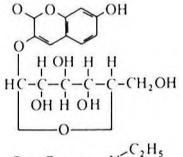	H_2O (pH ~ 9)	Blue 450–470 nm
7-Diethylamino-4-Methylcoumarin	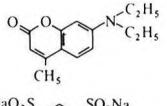	EtOH	Blue
Acetamidopyrene-trisulfonate	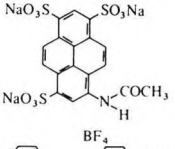	MeOH H_2O	Green-yellow
Pyrylium salt	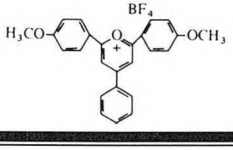	MeOH	Green

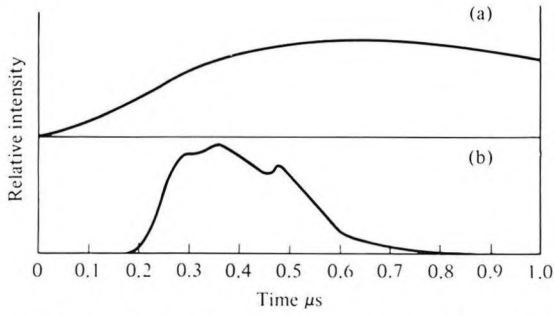

Figure 7-24 (a) Flashlamp pulse produced by a linear xenon flashlamp in a low-inductance circuit. (b) Laser pulse from a 10^{-3} molar solution of rhodamine 6G in methanol. (After Reference [23].)

in Figure 7-23, as an example, corresponds to a width of $\Delta\nu \simeq 1000\ \text{cm}^{-1}$. One elegant solution for realizing this tuning range [25] consists of replacing one of the laser mirrors with a diffraction grating, as shown in Figure 7-25. A diffraction grating has the property that (for a given order) an incident beam will be reflected back *exactly* along the direction of incidence, provided

$$2d \cos \theta = m\lambda \qquad m = 1, 2, \ldots \tag{7.9-1}$$

where d is the ruling distance, θ is the angle between the propagation direction and its projection on the grating surface, λ is the optical wavelength in the medium next to the grating, and m is the order of diffraction. This type of operation of a grating is usually referred to as the Littrow arrangement. When a grating is used as one of the laser mirrors, it is clear that the oscillation wavelength will be that which satisfies (7.9-1), since other wavelengths are not reflected along the axis of the optical resonator and will consequently "see" a very lossy (low-Q) resonator. The tuning (wavelength selection) is thus achieved by a rotation of the grating. It follows also that any other means of introducing a controlled, wavelength-dependent loss into the optical resonator can be used for tuning the output.

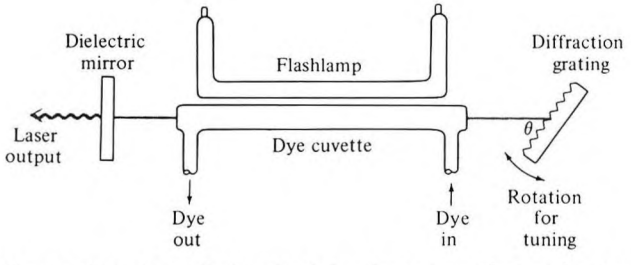

Figure 7-25 A typical pulsed dye laser experimental setup employing a linear flashlamp and a wavelength-selecting diffraction-grating reflector.

7.10 HIGH-PRESSURE OPERATION OF GAS LASERS

Consider a laser medium with an inversion density of ΔN atoms/m^3 at some transition with energy spacing near $h\nu_0$. If this medium is to be used as an amplifier of a pulsed signal at ν_0, then the maximum energy that can be extracted by the signal, through stimulated emission, is $\sim\Delta N h\nu_0$ joules per unit volume of the laser medium. It would follow straightforwardly that to increase the energy gain (= energy out/energy in) of the amplifier we need to increase the inversion density ΔN which, according to (6.4-5), can be done by stronger pumping.

Unfortunately, a mere increase in the pumping strength will increase, according to (5.6-10), the unsaturated gain $\gamma_0(\nu_0)$ of the medium, which will lead at some point to parasitic oscillation off spurious reflections or to energy depletion by amplification of the spontaneous emission [27].

One way around this problem in gas lasers is to increase the density (and pressure) of the amplifying medium. The increase in molecular density causes a proportionate decrease in molecular collision time τ which, according to (5.1-8), causes the transition linewidth $\Delta\nu$ to increase. At a given inversion, this would cause, according to (5.6-10), a reduction in the gain [recall here that $g(\nu_0) = (\Delta\nu)^{-1}$]. Alternatively, if the maximum tolerable gain is $\gamma_{\max}$, the reduction in gain due to increased pressure makes it possible to increase the inversion ΔN (by increased pumping) relative to its low-pressure value, until the maximum allowable gain $\gamma_{\max}$ is achieved. This, as discussed above, leads to increased stored energy density that can be "milked" by the signal pulse.

Let us look, somewhat more formally, at the problem of operating a continuous gas laser oscillator at increased pressures. Much of the work in this field was done on CO_2 lasers so that the following discussion will refer to this particular system, although the considerations are quite general.

The transition linewidth of the mixture of CO_2 and other gases used in CO_2 lasers can be written according to (5.1-8) as

$$\Delta\nu = \Delta\nu_D + \sum_i \frac{1}{\pi\tau_i} \tag{7.10-1}$$

where $\Delta\nu_D$ is the Doppler linewidth (5.1-15) and τ_i is the mean collision lifetime of a CO_2 molecule with a molecule of the ith molecular species (N_2, He, and so on) present in the mixture.

For a large range of pressures, τ_i^{-1} is proportional to the pressure [28] so that once $\Sigma_i(\pi\tau_i)^{-1} > \Delta\nu_D$, the transition linewidth $\Delta\nu$ is essentially proportional to pressure. This region is referred to as the *pressure-broadened regime* and is illustrated by Figure 7-26.

Consider now the problem of maintaining the laser oscillation in a high-pressure discharge. First, to achieve a given gain (that is equal to the resonator loss) we need, according to (5.6-10), to increase the inversion density

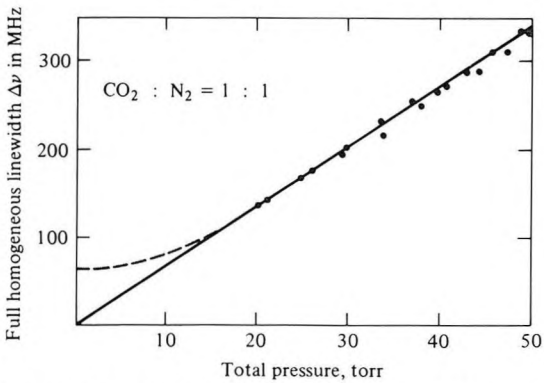

Figure 7-26 The 10.6 μm transition linewidth versus pressure for a gas mixture with equal partial pressures of CO_2 and N_2 at 300 K.

by an amount proportional to the pressure P in order to compensate for the increase of $\Delta\nu$.[7] Second, since the lifetime t_2 in the upper laser level varies as P^{-1}, the pumping power per molecule increases, according to (6.3-4), as P. The result is that the pumping power, for a given gain, increases as P^2. It follows that the output power, along with the excitation power, increases with P^2. This conclusion follows more formally, from (6.5-10), for the power output

$$P_0 = \frac{8\pi n^2 h\nu\Delta\nu A}{\lambda^2(t_2/t_{\text{spont}})}\, T\left(\frac{g_0}{L_i + T} - 1\right)$$

since $\Delta\nu \propto P$ and $t_2 \propto 1/P$.

[7] Recall here that in (5.6-10) $g(\nu_0) = (\Delta\nu)^{-1}$.

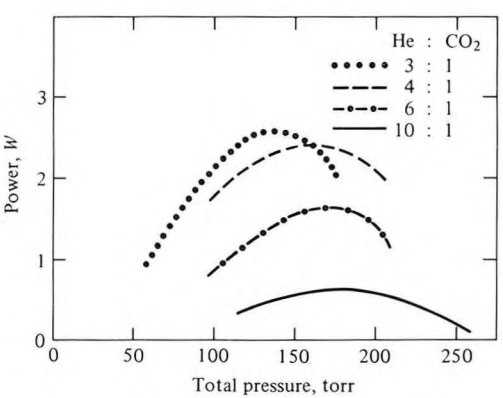

Figure 7-27 Output power versus total pressure under optimum pumping for He:CO_2 mixtures. (After Reference [29].)

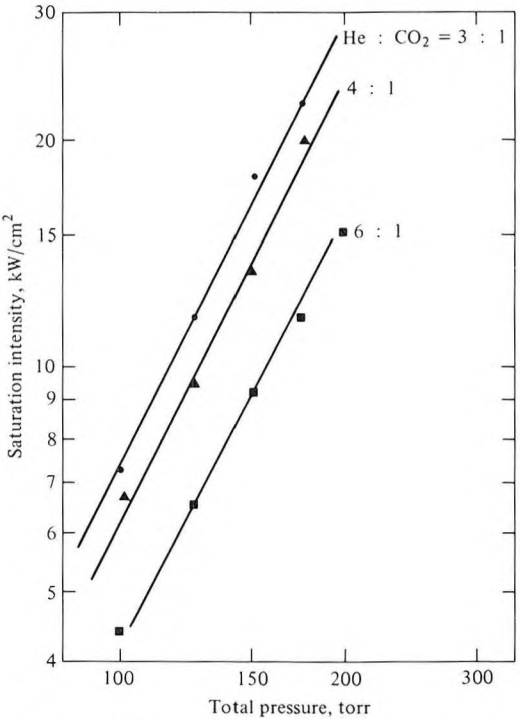

Figure 7-28 Measured saturation intensity versus pressure in a CO_2 laser. (After Reference [29].)

The increase of power with pressure is seen in Figure 7-27. The roll-off near $P = 150$ torr reflects the reduction in gain at the higher pressures. A more fundamental measure of the pressure effects is the variation of the saturation intensity (5.6-9)

$$I_s = \frac{8\pi n^2 \Delta\nu h\nu}{(t_2/t_{\text{spont}})\lambda^2}$$

that, for the reasons given above, should increase as P^2. Experimental data of I_s versus P is shown in Figure 7-28.

High-energy pulsed operation of CO_2 lasers [30] at atmospheric pressure has been responsible for large and simple lasers suitable for many industrial uses.

7.11 THE *Er*-SILICA LASER

One of the most important laser systems is that of *Er*-doped silica fibers [31–36] at $\lambda = 1.55$ μm. Such fibers pumped at $\lambda = 0.98$ μm or $\lambda = 1.48$ μm are used as in-line optical amplifiers in optical communication system and have major system implications [33]. They are discussed in detail in Section 11.11.

Problems

7-1 Derive the expression relating the absorption cross section at ν in a given $a \rightarrow b$ transition to the spontaneous $b \rightarrow a$ lifetime.

7-2 Derive condition (7.9-1) for the Littrow arrangement of a diffraction grating for which the reflection is parallel to the direction of incidence.

7-3

a. Estimate the exponential gain coefficient $\gamma(\nu_0)$ of a 10^{-4} molar solution of rhodamine 6G in ethanol by assuming the peak emission cross section to be comparable to the peak absorption cross section. Use the data of Figure 7-23.
b. Estimate the spontaneous lifetime for an $S_1 \rightarrow S_0$ transition.
c. Estimate the CW pump power threshold assuming 50 percent absorption of pump and 100 percent pumping quantum efficiency.

References

1. Maiman, T. H., "Stimulated optical radiation in ruby masers," *Nature* 187:493, 1960.
2. Maiman, T. H., "Optical and microwave-optical experiments in ruby," *Phys. Rev. Lett.* 4:564, 1960.
3. Cronemeyer, D. C., "Optical absorption characteristics of pink ruby," *J. Opt. Soc. Am.* 56:1703, 1966.
4. Schawlow, A. L., "Fine structure and properties of chromium fluorescence." In *Advances in Quantum Electronics*, J. R. Singer, ed. New York: Columbia University Press, p. 53, 1961.
5. Yariv, A., "Energy and power considerations in injection and optically pumped lasers," *Proc. IEEE* 51:1723, 1963.
6. Geusic, J. E., H. M. Marcos, and L. G. Van Uitert, "Laser oscillations in Nd-doped yttrium aluminum, yttrium gallium and gadolinium garnets," *Appl. Phys. Lett.* 4:182, 1964.
7. Kushida, T., H. M. Marcos, and J. E. Geusic, "Laser transition cross section and fluorescence branching ratio for Nd^{3+} in yttrium aluminum garnet," *Phys. Rev.* 167:1289, 1968.
8. Snitzer, E., and C. G. Young, "Glass lasers." In *Lasers*, vol. 2, A. K. Levine, ed. New York: Marcel Dekker, Inc., p. 191, 1968.
9. Javan, A., W. R. Bennett, Jr., and D. R. Herriott, "Population inversion and continuous optical maser oscillation in a gas discharge containing a He–Ne mixture," *Phys. Rev. Lett.* 6:106, 1961.
10. White, A. D., and J. D. Rigden, "Simultaneous gas maser action in the visible and infrared," *Proc. IRE* 50:2366, 1962.
11. Bennett, W. R., "Gaseous optical masers," *Appl. Opt., Suppl. 1, Optical Masers*, p. 24, 1962.
12. Patel, C. K. N., "Interpretation of CO_2 optical maser experiments,"

Phys. Rev. Lett. 12:588, 1964; also, "Continuous-wave laser action on vibrational rotational transitions of CO_2," *Phys. Rev.* 136:A1187, 1964.

13. Herzberg, G. H., *Spectra of Diatomic Molecules*. Princeton, N.J.: Van Nostrand, 1963.
14. Patel, C. K. N., "High power CO_2 lasers," *Sci. Am.* 219:22, Aug. 1968.
15. Bridges, W. B., "Laser oscillation in singly ionized argon in the visible spectrum," *Appl. Phys. Lett.* 4:128, 1964.
16. Gordon, E. I., E. F. Labuda, and W. B. Bridges, "Continuous visible laser action in singly ionized argon, krypton and xenon," *Appl. Phys. Lett.* 4:178, 1964.
17. Stevens, B., and E. Hutton, *Nature* 186:1045, 1960.
18. Rokni, M., J. Jacob, and J. Mangano, *Phys. Rev.* A16:2216, 1977.
19. Holzrichter, J. F., D. Eimerl, E. V. George, J. B. Trenholme, W. W. Simmons, and J. T. Hunt, "High Powered Lasers," *J. Fusion Energy* 2:5, 1982.
20. Hutchinson, M. H. R., "Excimers and Excimer Lasers," *Appl. Phys.* (Springer-Verlag) 21:95, 1980.
21. Stockman, D. L., W. R. Mallory, and K. F. Tittel, "Stimulated emission in aromatic organic compounds," *Proc. IEEE* 52:318, 1964.
22. Sorokin, P. P., and J. R. Lankard, "Stimulated emission observed from an organic dye, chloroaluminum phtalocyanine," *IBM J. Res. Dev.* 10:162, 1966.
23. Schafer, F. P., W. Schmidt, and J. Volze, "Organic dye solution laser," *Appl. Phys. Lett.* 9:306, 1966.
24. Snavely, B. B., "Flashlamp-excited dye lasers," *Proc. IEEE* 57:1374, 1969.
25. Soffer, B. H., and B. B. McFarland, "Continuously tunable, narrow band organic dye lasers," *Appl. Phys. Lett.* 10:266, 1967.
26. Peterson, O. G., S. A. Tuccio, and B. B. Snavely, "CW operation of an organic dye laser," *Appl. Phys. Lett.* 17:266, 1970.
27. Yariv, A., *Quantum Electronics*, 3d ed. New York: Wiley, 1989.
28. Taylor, R. L., and S. Bitterman, "Survey of vibrational and relaxation data for processes important in the CO_2–N_2 laser system," *Rev. Mod. Phys.* 41:26, 1969.
29. Abrams, R. L., and W. B. Bridges, "Characteristics of sealed-off waveguide CO_2 lasers," *IEEE J. Quant. Elec.* QE-9:940, 1973.
30. Beaulieu, J. A., "High peak power gas lasers," *Proc. IEEE* 59:667, 1971.
31. Simon J. C., "Semiconductor laser amplifier for single mode optical fiber communications," *J. Opt. Commun.* 4:51, 1983.
32. Mears, R. J., L. Reekie, I. M. Jauncey, and D. N. Payne, "Low noise Erbium-doped fiber amplifier operating at 1.54 mm," *Electron. Lett.* 23:1026, 1987.
33. Hagimoto, K. et al., "A 212 km non-repeatered transmission experiment at 1.8 Gb/s using LD pumped Er^{3+}-doped fiber amplifiers in an Im/direct-

detection repeater system." In *Proc. Opt. Fiber Conf., Houston, TX,* Postdeadline Paper PD15, 1989.

34. Olshansky, R., "Noise figure for Er-doped optical fibre amplifiers," *Elect. Lett.* 24:1363, 1988.

35. Payne, David N., "Tutorial session abstracts," *Optical Fiber Communication (OFC 1990) Conference*, San Francisco, 1990.

36. See, for example, Eisenstein, G., U. Koren, G. Raybon, T. L. Koch, M. Wiesenfeld, M. Wegener, R. S. Tucker, and B. I. Miller, "Large-signal and small-signal gain characteristics of 1.5 mm quantum well optical amplifiers," *Appl. Phys. Lett.* 56:201, 1990.